Environment Canada Environnement Canada

Canada

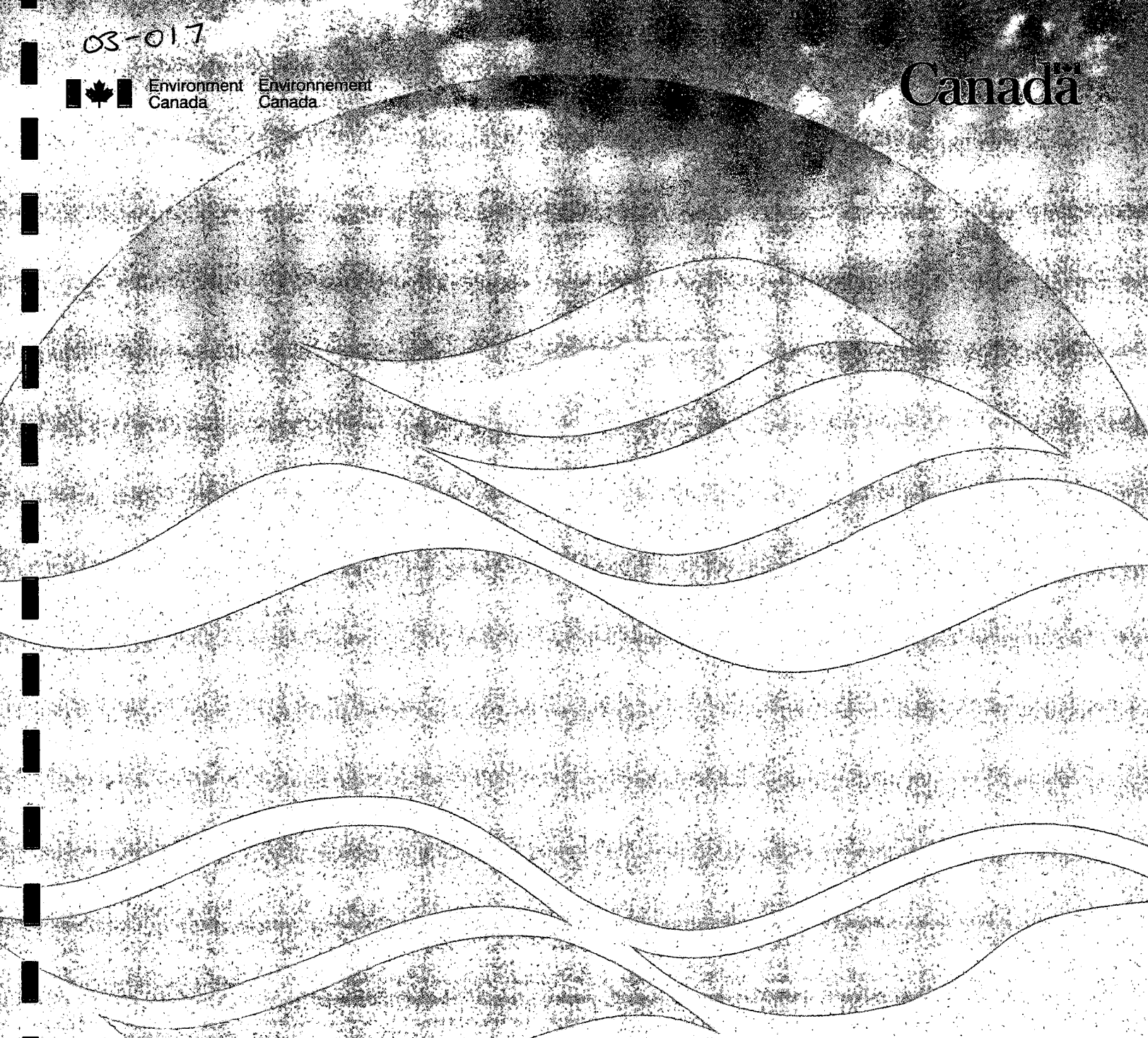

Wave generated fractures in river ice covers

by Spyros Beltaos

NWRI Contribution # 03-17

Available online at www.sciencedirect.com
SCIENCE DIRECT
ELSEVIER
Cold Regions Science and Technology 40 (2004) 179–191
cold regions science and technology
www.elsevier.com/locate/coldregions

Wave-generated fractures in river ice covers

Spyros Beltaos*

Aquatic Ecosystem Impacts Research Branch, National Water Research Institute, 867 Lakeshore Road, Burlington, Ontario L7R 4A6, Canada

Received 23 September 2003; accepted 29 July 2004

Abstract

The breakup of the ice cover in northern rivers is a brief but crucial event in the life cycle of many aquatic species and can trigger extreme ice jam events with major socio-economic impacts and significant climate change implications. An important, but vaguely understood, breakup process is the fracture of the winter ice cover by low-amplitude water waves. Previous work on this subject has been based on the assumption of an infinitely long wave propagating under an infinitely long and "edgeless" ice cover. This configuration does not account for structural constraints imposed by the proximity of an ice edge or a transverse crack. Consequently, it only furnishes approximate values of bending stresses, and tells little about the spacing of cracks that may be generated by an advancing wave, which is the only visual evidence that can identify the relevant fracture mechanism in the field. Herein, edge proximity is taken into account by making plausible simplifications to the ice response equation, and using wave forms of limited extent. It is shown that such conditions generally produce higher bending stresses than does the infinite wave/edgeless cover configuration. The distance of the peak bending stress from the edge, which defines the spacing of cracks, varies with wavelength and is less than 100 ice thicknesses or so. This is comparable to that of high-amplitude, single waves (or surges) that result from ice jam releases, but much less than fractures generated by bending on horizontal planes, caused by the meandering river plan form. Comparison of the present results with the limited available evidence indicates that wave-generated fractures occur during the passage of ice jam release surges.

Keywords: Crack spacing; Edge conditions; Fracture; Ice cover; River; Wave

1. Introduction

The breakup of the ice cover in northern rivers is a brief but crucial event in the life cycle of many aquatic species and can trigger extreme ice jam events with major socio-economic impacts. The need for physical understanding of river ice breakup processes, known to be intimately linked to hydroclimatic factors, is accentuated by the emerging issue of climate change. Predicting, and adapting to, climate impacts on the economy and on aquatic ecology, caused by alterations to ice breakup regimes, require a thorough and quantitative knowledge of the complex mechanisms that are at work. Of these, the mechanisms that govern the onset of breakup play a central role, and have been

* Tel.: +1 905 336 4898; fax: +1 905 336 4420.
E-mail address: Spyros.Beltaos@ec.gc.ca.

0165-232X/$ - see front matter
doi:10.1016/j.coldregions.2004.07.002

the object of many previous studies (e.g., see Beltaos, 1995, 1997).

In the past decade, it has been possible to depart from the empiricism of earlier works and derive a conceptual model that does not require site-specific historical data and can be applied to different sites with minimal calibration. The quantification of this model depends on the spacing of transverse cracks, which form after the appearance of longitudinal, near-bank fractures known as "hinge" cracks, and before the ice cover is set in motion (Beltaos, 1997). Typically, transverse cracks are spaced a few river widths, or hundreds of metres or kilometers, apart, and can be explained by flexure due to bending on horizontal planes (Beltaos, 1990, 1998).

Flexural stresses can also be induced by vertical bending of the ice cover, resulting from large curvature of the water surface, when the latter is disturbed by waves. A well-known wave that forms during the breakup process is the surge that follows the release of an ice jam. This is a single wave that can attain a height of a few metres (e.g., Henderson and Gerard, 1981; Beltaos and Krishnappan, 1982; Hicks, 2003). Its ice-fracturing capacity results from the abruptness of the wave front. It has been calculated that a steep surge (slope over ~0.005) can fracture the ice cover and produce transverse cracks spaced at tens of ice thicknesses (Billfalk, 1982; Beltaos, 1985, 1990).

More recently, Daly (1995) showed that significant vertical bending can also be induced by much shorter, low-amplitude waves traveling under an ice cover. Even with amplitude of mere centimeters, considerable bending stresses can develop at wave peaks and troughs, where the curvature is large. This type of stressing has also been proposed as a mechanism that can generate transverse fractures in a river ice cover (Daly, 1993, 1995; Xia and Shen, 1999, 2002). The sources of low-amplitude waves cannot be positively identified at present, but they have to originate at water surface disturbances of various types. These may include surges and breaking fronts that attend ice jam releases, reservoir releases, or even brief movements of individual ice sheets.

Although the theoretical side of this question is fairly advanced, there is hardly any experimental or observational evidence that can be used to test various theories. Ordinary water level recording gauges do not have the fine resolution that is required to register such short waves, whose period may be in the order of a minute. Using specially designed pressure-sensing and recording equipment, Beltaos and Rowsell (2001) did register numerous small waves (amplitude=a few centimeters) during the prebreakup period on the Southwest Miramichi River, NB, but their periods, and hence wavelengths, were far too large for development of significant bending stresses in the ice cover.

At present, therefore, identification of the mechanism responsible for transverse fractures has to be primarily based on their observed spacing. Although it has been thought that the spacing is equal to the wavelength (Xia and Shen, 1999, 2002), this question appears to merit further attention. In previous analyses, it is assumed that water waves propagate under an infinitely long, uncracked ice cover. This assumption does not take into account the well-known conditions of zero bending moment and shearing force that must be fulfilled at the edge of a real ice cover, or at an existing crack. The same holds for cracks that may be generated by the advancing wave: When the first crack forms, the local bending moments and shearing forces will vanish, thus producing a new "edge" condition and altering the local variation of the bending moment. This process is repeated as the wave moves downstream (or upstream) and thus governs the distance between successive cracks. It is difficult to see why this distance should be equal to the length of the wave. Moreover, adherence of the ice response to the edge conditions will alter the local bending moment (and flexural stress) distribution. The ice-fracturing capacity of a wave may thus be very different from what has been previously calculated.

The flexure of an ice cover by a low-amplitude wave is examined herein by treating the cover as a semi-infinite beam that deforms when a water wave arrives and propagates under it. The bending moment and shearing force are set to zero at the edge of the cover, and the locations of maximum bending moments are derived via approximate solutions of the differential equation describing the deformation of the ice in response to the water wave. The results indicate that the edge has a large influence on the ice response wave and attendant flexural stresses, while suggesting that crack spacing can only be in the order of tens of ice thicknesses.

2. Background information

The propagation of water waves under an ice cover has been studied by numerous investigators, especially for deep-water, sea ice applications (e.g., see Balmforth and Craster, 1999). For ice-covered rivers, Daly (1993, 1995) presented a mathematical analysis that was further refined in a discussion by Steffler and Hicks (1994). Assuming sinusoidal water and flexural waves propagating in phase under and within an infinitely long ice cover, Daly linearized the equations of motion and determined the wave celerity as a function of channel characteristics and ice properties. This variation is illustrated in Fig. 1 where the celerity

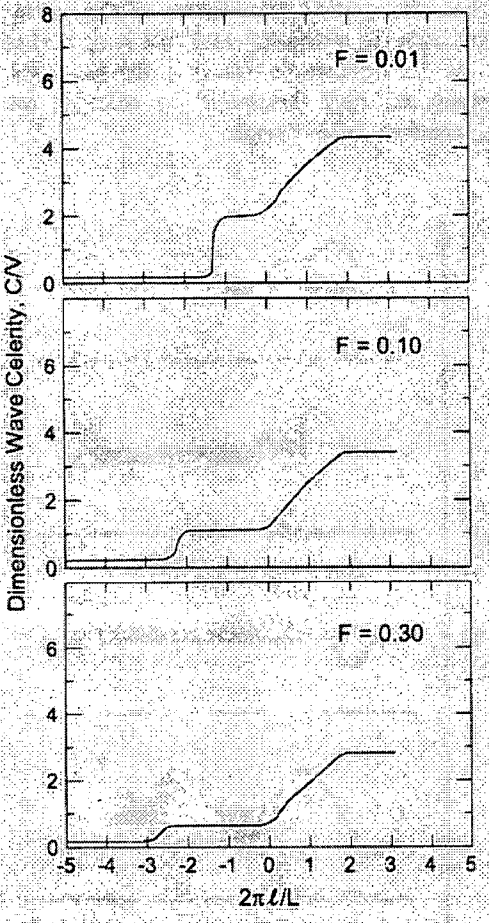

Fig. 1. Variation of wave celerity with dimensionless wave number (after Daly, 1995, with changes). Logarithmic scale is used on both axes.

C is normalized by the average unperturbed flow velocity V and plotted against the dimensionless wave number, defined as $2\pi l/L$ (l=characteristic ice length, defined later; L=wavelength). In Fig. 1, F is Froude number while the modulus of elasticity of ice E, river slope S, ice cover thickness h, and unperturbed water depth are assumed to be equal to 5 GPa, 0.0005, 0.5 m, and 5 m, respectively.

A different behaviour is exhibited within different ranges, or "bands," depending on wavelength, river slope, and flow depth. The first band comprises very small wave numbers (or very large wavelengths L) and is known as the *kinematic* band. Here, gravitational and frictional forces are dominant, while the celerity C is constant and approximately equal to 1.5 V. Kinematic waves propagate only in the downstream direction (Ponce and Simons, 1977). In the second or *dynamic* band, C increases with wave number as inertial forces also play a role. Inertial and gravitational forces dominate the third, or *gravity*, band. The celerity is again constant but much higher than the kinematic value:

$$C = |V \pm \sqrt{gy}| \quad \text{(gravity band)} \tag{1}$$

in which V and y are average velocity and depth, respectively, of unperturbed flow; and g is gravitational acceleration. The plus and minus signs in Eq. (1) correspond to waves that propagate in the downstream and upstream directions, respectively.

The gravity band is followed by the *ice-coupled* band, where gravitational, inertial, and ice-bending forces predominate. The celerity increases with increasing wave number in the ice-coupled band, and becomes a constant in the final, or *acoustic*, band. In the first three bands, C does not depend on ice properties, thus behaving much as it would in an open channel (see also Ponce and Simons, 1977). Steffler and Hicks (1994) calculated that ice coupling begins to have an effect on the wave celerity when the wavelength drops below a limiting value of $16.7l/(1+F)^{1/4}$, which translates to $2\pi l/L > 0.38(1+F)^{1/4}$. This is also evident in Fig. 1, although large deviations from the open water celerity do not become apparent until $2\pi l/L$ exceeds 1 or so.

Daly (1995) also investigated the conditions under which an ice cover could be fractured by water waves.

This was done in terms of the characteristic length of the ice cover l, which is herein defined as:

$$l = \sqrt[4]{\frac{Eh^3}{12\gamma}} \quad (2)$$

in which h is ice cover thickness and γ is unit weight of water. The ice cover is assumed to respond as a beam rather than as a plate, which is the likely condition once hinge cracks have formed and the water level has risen sufficiently to effect full hinge separation. On the other hand, if a plate condition were assumed, as is sometimes found in the literature, the term $1-\nu^2$ (ν=Poisson ratio) will also appear on the denominator of the fraction in Eq. (2). From a practical point of view, the difference in the present case is trivial because $(1-\nu^2)^{1/4}$ is very close to 1 ($\nu \approx 0.33$ for ice). When typical values for E (7 GPa) and γ (9810 N/m^3) are substituted in Eq. (2), the result is (Gold, 1971):

$$l \approx 16h^{3/4} \quad (l \text{ and } h \text{ in meters}) \quad (3)$$

Daly's (1995) analysis resulted in the following conclusions:

- Long waves ($L/l \gg 2\pi$, or $2\pi l/L \ll 1$) are not very effective in fracturing the ice cover, which is consistent with the results of Billfalk (1982) and Beltaos (1990), who had ignored (as small) the effect of the vertical ice acceleration on flexure.
- Short waves ($L/l \ll 2\pi$, or $2\pi l/L \gg 1$) are also ineffective in fracturing an ice cover.
- Wavelengths near $2\pi l$ ($2\pi l/L \sim 1$) are the most effective, being capable of fracturing the ice cover even with moderate amplitude (e.g., 0.05–0.20 m). The wave period associated with this range of L is estimated to be between 0.2 and 20 s.

More recently, Xia and Shen (1999, 2002) presented a theoretical analysis of nonlinear waves and concluded that highly asymmetrical "cnoidal" waves would be more effective in fracturing the ice cover than sinusoidal ones of comparable wavelength. This is not surprising because cnoidal waves are characterized by brief, sharp troughs separated by prolonged, flat peaks. Theoretically derived wavelengths were in the order of hundreds of metres.

As already indicated, these theories assume an infinitely long, uncracked ice cover and do not account for the edge conditions of zero moment and shear. Moreover, no consideration is given to the fact that the waves propagate in the downstream or upstream direction, which is the likely reason for equating crack spacing to wavelength. The actual situation is depicted in Fig. 2.

A water wave arrives at the edge of an ice cover at time t_0 and progressively moves into the ice-covered reach as time increases. From a structural standpoint, the edge may also be an existing or newly formed crack. The wave outline is highly exaggerated in the vertical direction and represents the variation of the phreatic water level, multiplied by the unit weight of water, the vertical coordinate of the wave also represents the distributed load that is applied on the cover. In response to this load, the ice cover will deform and may fracture if the resulting bending moments are large enough.

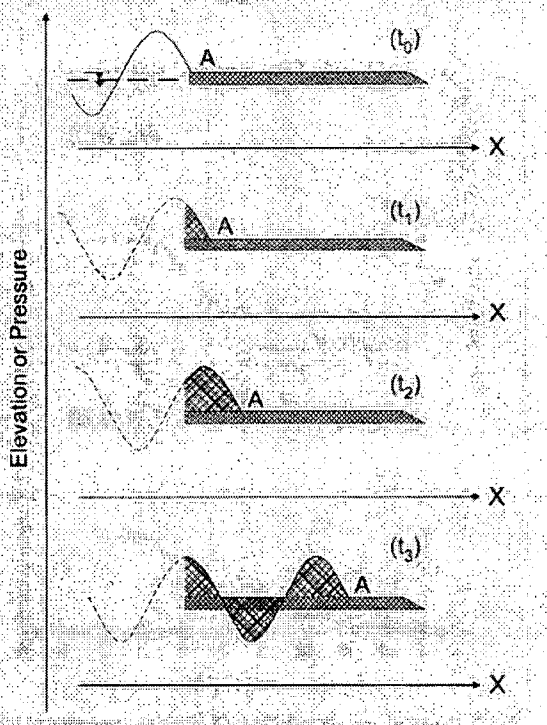

Fig. 2. Schematic illustration of the progressive advance of a water wave into an ice-covered reach.

Intuition suggests that the bending moment will peak at about time t_2 or later, when one or two wave peaks (or troughs) have gone past the edge, and the ice is forced to rise and bend with the wave. As soon as a crack forms, a new edge is created and the process is repeated. In this manner, cracks will form sequentially, in step with the advancing wave, and their spacing will be governed by both the flexural characteristics of the ice cover and the characteristics of the wave. The mechanism shown in Fig. 2 can be quantified in an approximate manner, as described next.

3. Analysis

3.1. Problem formulation

Consider an ice cover that has been separated from the river banks via hinge cracking. The partial differential equation describing ice deformation η in response to a laterally uniform water wave propagating under the ice cover is (Daly, 1995):

$$\frac{s_i h}{g}\frac{\partial^2\eta}{\partial t^2} + l^4\frac{\partial^4\eta}{\partial x^4} + \eta = w \tag{4}$$

in which s_i=specific gravity of ice; x=distance along the river; t=time; and w=the perturbation of the phreatic surface, which, under conventional linearization assumptions, can be shown to be a sinusoidal function, i.e.,

$$w = w_0\cos(kx - \omega t) \tag{5}$$

with k=wave number=$2\pi/L$; $\omega=2\pi/T$, and L, T=wavelength and wave period, respectively. The wave celerity C is then equal to L/T. For an infinitely long ice cover, Daly (1995) showed that the ice response wave (or "ice wave" for short) is obtained by substituting Eq. (5) into Eq. (4) to find:

$$\eta = \eta_0\cos(kx - \omega t) \tag{6}$$

while the ice wave amplitude is given by:

$$\eta_0 = \varepsilon w_0 \tag{7}$$

Here, ε is a coefficient that depends on the dimensionless wave number, $2\pi l/L$ (=kl). In the range kl<0.5, $\varepsilon \approx 1$; as kl increases beyond 0.5, ε decreases, taking the value of ~0.5 at kl=1 and becoming much less than 1 for kl>5. This variation implies that long water waves (small kl) generate nearly identical ice response while the cover hardly responds to short water waves (large kl).

Noting that the bending moment and shearing force generated within the ice cover vary in proportion to $\partial^2\eta/\partial x^2$ and $\partial^3\eta/\partial x^3$, respectively, it can be shown that the sinusoidal wave represented by Eq. (6) cannot satisfy the structural edge conditions, for any pair of values of x and t. Consequently, Eq. (6) does not apply in the vicinity of an edge or crack.

An approximate solution that satisfies the edge conditions can be obtained by first simplifying Eq. (4). Using Eq. (6) for an order-of-magnitude analysis, it is possible to calculate each of the terms on the left-hand side (LHS) of Eq. (4), and hence to assess the relative magnitude of the inertial term:

$$r = \left|\frac{\frac{s_i h}{g}\frac{\partial^2\eta}{\partial t^2}}{l^4\frac{\partial^4\eta}{\partial x^4} + \eta}\right| = \frac{s_i h v}{l^2}\frac{C^2}{gy}\frac{(kl)^2}{1+(kl)^4} \tag{8}$$

Noting that l is in the order of 10 m for typical river ice thickness, and using Daly's findings regarding the celerity C (Fig. 1), it can be shown that $r \ll 1$ for all values of kl, with the possible exception of the upper end of the ice-coupled band (where flexural stresses are far too small to cause fracture). Consequently, Eq. (4) reduces to:

$$l^4\frac{\partial^4\eta}{\partial x^4} + \eta \approx w \tag{9}$$

This simplification has been derived by assuming linear waves of sinusoidal form. An order-of-magnitude analysis has further shown (Appendix A) that it is valid for any type of wave whose celerity has the magnitude indicated in Fig. 1. This finding includes the cnoidal wave, whose celerity is close to that of the gravity wave (Xia and Shen, 1999, 2002).

Eq. (9) represents the response of an elastic beam resting on an elastic foundation (Hetenyi, 1946). The reaction per unit area is equal to the local ice deflection times the unit weight of water γ. The beam

is subjected to a distributed load, equal to γw, and pointing upward when the phreatic water surface is above the undisturbed water surface (see also Fig. 2).

The proximity of the edge is taken into account by stipulating the following boundary conditions:

$$\frac{\partial^2\eta}{\partial x^2}=0 \text{ and } \frac{\partial^3\eta}{\partial x^3}=0 \text{ at } x=0, \text{ for any value of } t \tag{10}$$

3.2. Solution for infinitely long water wave: uncracked cover

It is useful to consider first the case of an infinitely long wave that is propagating under a semi-infinite ice cover, and described by Eq. (5) at all values of x and t. This situation can only arise if the wave is not sufficiently steep to cause fracture, so that successive wave forms can move past the actual ice edge without changing the location of the point where the "edge conditions" must be applied.

It can be verified by direct substitution that the solution to Eq. (9), subject to the boundary conditions of Eq. (10) and with w given by Eq. (5), is:

$$\frac{\eta}{w_0}=\frac{4}{4+\beta^4}\cos(\beta\xi-\tau) - \frac{2\beta^2}{4+\beta^4}e^{-\xi}[\sin\xi\cos\tau-\cos\xi(\beta\sin\tau+\cos\tau)] \tag{11}$$

in which

$$\xi=x/\sqrt{2}l;\quad \tau=\omega t=2\pi t/T;\qquad \beta=\sqrt{2}kl=2\pi l\sqrt{2}/L \tag{12}$$

The first term on the right-hand side (RHS) of Eq. (11) is the response of the ice cover very far from the edge ($\xi\rightarrow\infty$), whereas the second term describes effects arising from the proximity of the edge. The ultimate ($\xi\rightarrow\infty$) amplitude of the ice response is seen to be nearly equal to the amplitude of the water wave, so long as L/l is greater than about 13, but quickly diminishes as L decreases and the coefficient β increases.

The variation of the stress generated in the ice cover can be explored by taking the second spatial derivative of Eq. (11) and rearranging to obtain [after setting the flexural stress equal to $-(Eh/2)(\partial^2\eta/\partial x^2)$]:

$$\frac{l^2}{hw_0}\frac{\sigma}{E}=S=\frac{\beta^2}{4+\beta^4}(\cos(\beta\xi-\tau) - e^{-\xi}[\cos\xi\cos\tau+\sin\xi(\beta\sin\tau+\cos\tau)]) \tag{13}$$

in which S is the dimensionless stress defined on the LHS of the equation. Positive stress values represent tension in the top half of the cover. Because ice is weaker in tension than in compression, cracks can only be generated by tensile stresses. Negative values of σ imply that tension occurs in the bottom half of the cover, so that the tensile, or bending, stress is equal to $|\sigma|$. Eq. (13) suggests that the bending stress is proportional to the amplitude of the water wave, while its dependency on E and h is not obvious because β and l also depend on these parameters. Very important is the influence of the wavelength [recall from Eq. (12) that $\beta=\sqrt{2}kl$]. For long waves (small kl), the stress varies in inverse proportion to the square of L, and tends to zero as L increases. For short waves, σ increases in direct proportion to L^2 and again tends to zero as L decreases (and kl increases). The highest stresses occur when $kl\sim1$, which is in accord with Daly's (1995) findings.

3.3. Solution for a wave propagating into an undisturbed region of the channel

The results presented in the previous section apply so long as the bending stresses remain lower than the flexural strength of the ice, and no cracks form. Otherwise, the distributed load that is applied on the beam at any given time will not involve the entire semi-infinite water wave ($x=0-\infty$) but only the portion that has advanced far enough past the edge (or crack) to cause fracture (Fig. 2). Physically, this situation describes a finite wave propagating into an undisturbed region of the channel. Mathematically, it can be regarded as a "truncated" wave, relative to the semi-infinite wave discussed in the previous section. For the sake of brevity, the term "truncated wave" (TW) will be used in subsequent text to denote a wave propagating into an undisturbed region of the channel. The "truncation" should be understood to apply to the

horizontal extent of the wave rather than to its amplitude.

Rigorous mathematical solution of this problem is impractical, owing to the multitude of distributed load configurations that would have to be considered in order to investigate adequate ranges of kl and τ values. Instead, a simpler method is utilized, based on superposition of ice response to several concentrated loads. Considering a concentrated load P located a distance a from the edge, Hetenyi (1946) has calculated the bending moment M as:

$$m \equiv 2\sqrt{2}\frac{M}{Pl} = e^{-\xi}[\mu_1(\cos\xi - \sin\xi) - 2\mu_2\cos\xi] + e^{-|\alpha-\xi|}[\cos|\alpha - \xi| - \sin|\alpha - \xi|] \quad (14)$$

in which

$$\alpha = a/\sqrt{2}l; \quad \mu_1 = e^{-\alpha}(3\cos\alpha - \sin\alpha); \quad \mu_2 = e^{-\alpha}(2\cos\alpha - \sin\alpha) \quad (15)$$

A distributed load, such as the one imposed by the TW form shown in Fig. 2, can be subdivided into parts and replaced by j concentrated loads, with j being a large number. Eq. (14) can then be applied to each load and the results superposed linearly (since Eq. (4) is linear) to determine the bending moment that corresponds to the distributed load. Individual loads P_k are calculated as:

$$P_k = \gamma w_0\sqrt{2}l\langle w/w_0\rangle_k\Delta\xi_k \quad (16)$$

in which the symbol $\langle\rangle_k$ stands for average value over the kth interval of ξ, which is in turn represented by $\Delta\xi_k$. The load P_k is assumed to act at the center of the interval, and it produces a moment M_k that can be computed via Eq. (14) after inserting appropriate values of the coefficients defined in Eq. (15). The total moment M_T is then given by:

$$M_T = \frac{l}{2\sqrt{2}}\sum_1^j P_k m_k = \frac{l\gamma w_0\sqrt{2}l}{2\sqrt{2}}\sum_1^j \langle w/w_0\rangle_k\Delta\xi_k m_k = \frac{l^2\gamma w_0}{2}\sum_1^j \langle w/w_0\rangle_k\Delta\xi_k m_k \quad (17)$$

Substituting $M=\sigma h^2/6$ gives further:

$$\frac{l^2}{hw_0}\frac{\sigma}{E} \equiv S = \frac{1}{4}\sum_1^j \langle w/w_0\rangle_k\Delta\xi_k m_k \quad (18)$$

To facilitate the computation, an EXCEL spreadsheet has been generated, which calculates the combined moment caused by 20 consecutive loads. The loads and their corresponding locations are determined from the shape of the wave form (Eq. (5)), truncated at the point where the water surface just begins to rise from its undisturbed elevation ($w=0$ and $\partial w/\partial x<0$). Different values of τ produce different degrees of advancement past the edge of the cover (Fig. 2).

4. Results

Fig. 3a and b compares ice responses to different water waves that have advanced for an infinite distance past the edge of the ice cover. As already mentioned, this can only happen if the generated bending moments are at all times insufficient to fracture the cover, so that the edge location remains fixed. As predicted by Daly (1995), short water waves (large kl) produce a subdued ice response, whereas the ice cover responds much more readily to longer waves. The ice and water waves tend toward complete identity as the wavelength increases and kl decreases to below ~0.5. Regardless of length, the two waves are in phase, except near the edge, where the boundary conditions predominate.

More interesting is the variation of the dimensionless stress S when the water wave is truncated to represent different stages of advancement past the edge (as shown in Fig. 2). Fig. 4a illustrates the results of the superposition method for a short wave (kl=2) that has advanced into the ice-covered reach by a distance of nearly a wavelength. The full-wave (FW) solution (Eq. (13)) is also shown for comparison. It closely matches the stress generated by the TW between the ice edge and the point of the first peak.

The peak bending stress caused by the TW occurs close to the edge and is higher than the peak stress generated by the FW at large values of ξ, where the influence of the edge is negligible. The latter is the

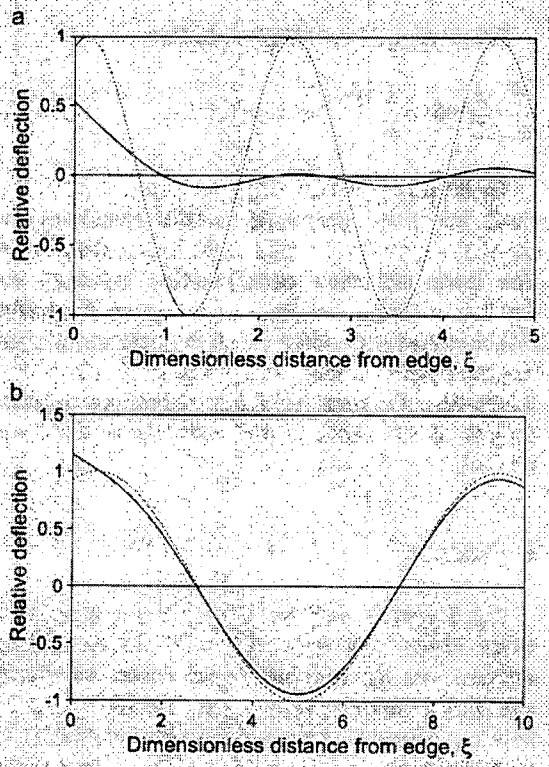

Fig. 3. (a) Ice response (solid line) to a short water wave (dashed line): kl=2.0, $\tau=\pi/8$. (b) Ice response (solid line) to a medium-length water wave (dashed line): kl=0.5, $\tau=\pi/8$. Relative deflection represents η/w_0 and w/w_0, respectively.

same as the peak moment caused by an FW propagating under an infinite ice cover that has no edge. This has proved to be a general feature of TWs, regardless of wavelength, and is evidently caused by the proximity of the edge. Another general characteristic of the TW moment distribution is the presence of a partial peak that occurs beyond the point of truncation (i.e., the leading edge of the TW). Although unimportant in the case depicted in Fig. 4a, this peak becomes increasingly significant as the wavelength increases.

This is illustrated in Fig. 4b, depicting the case of an intermediate wavelength. Here, the "frontal" peak, which occurs past the leading edge of the TW, is still smaller than the edge-controlled peak (occurring at ξ=4) but comparable in magnitude. Inaccuracies associated with load discretization in the superposition method are now apparent in the oscillating form of the TW curve, and result from the increasing separation between the concentrated loads.

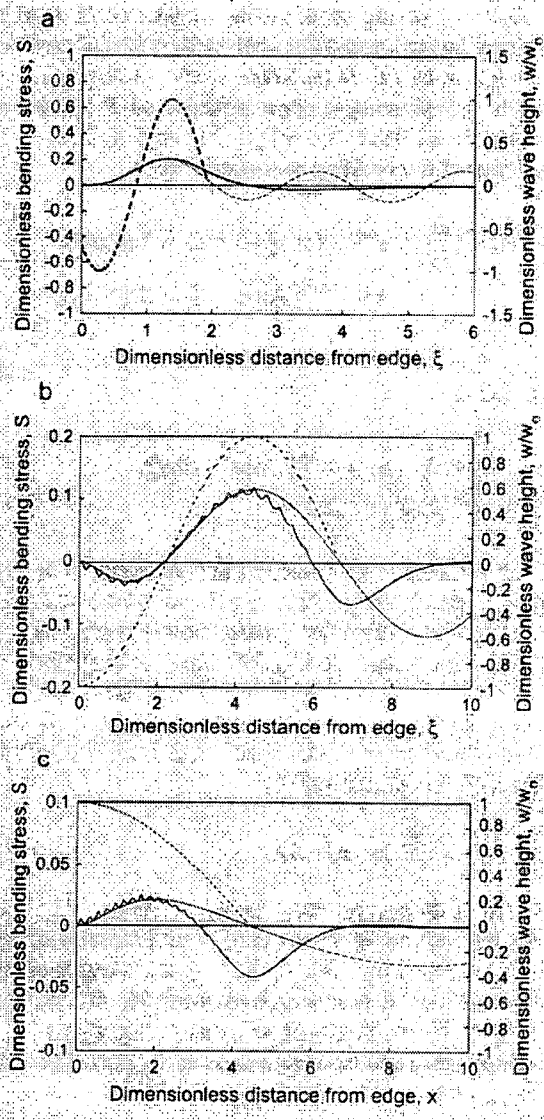

Fig. 4. (a) Stress variation (solid line) caused by a truncated water wave (dotted line) with kl=2.0 and $\tau=5\pi/4$. (b) Stress variation (solid line) caused by a truncated water wave (dotted line) with kl=0.5 and $\tau=\pi$. (c) Stress variation (solid line) caused by a truncated water wave (dotted line) with kl=0.25 and τ=0. The dashed line represents the stress variation caused by the full wave (Eq. (13)).

Below a value of kl=0.34, the frontal peak exceeds the edge-controlled value and occurs very near the leading edge of the TW (Fig. 4c). The magnitude of this peak is insensitive to the value of τ, once the latter is zero or positive. In this range (kl<0.34) therefore, the wave only needs to advance past the edge by a quarter of the wavelength (τ=0) in order to attain its maximum bending stress. This finding is akin to the results obtained by Billfalk (1982) for monoclinal waves of linear front. Moreover, the peak dimensionless stress $|S_p|$ varies now in direct proportion to kl, i.e.,

$$|S_p| \approx 0.16kl \quad \text{(for } kl<0.34\text{)} \tag{19}$$

Recalling the definition of S and substituting $k=2\pi/L$, Eq. (19) can also be rewritten as:

$$\sigma \approx 0.25E\frac{w_0}{(L/4)}\frac{h}{l} \quad \text{(for } kl<0.34\text{)} \tag{20}$$

which indicates that the stress is proportional to the average wave slope, expressed by the quantity $w_0/(L/4)$. In terms of wave slope, Billfalk's (1982) result for long triangular loads is similar to Eq. (20), but the numerical coefficient is 0.18 instead of 0.25.

As illustrated in Fig. 4a–c, the highest bending moments occur when the wave has advanced past the edge by a quarter of the wavelength when kl<0.34, and close to one wavelength at higher values of kl, being 1.25 wavelengths at kl=1. In terms of actual distance form the edge, the largest such advance was found for kl=0.5 and amounted to 9.5l.

5. Ice cover fracture and crack spacing

The variation of the peak stress with wavelength is summarized in Fig. 5, where the symbol S_p is used to denote the peak *absolute* value of S (see Eq. (13)), since only tensile stresses are considered. The relative fracture effectiveness of medium-length waves, first shown by Daly (1995) for the full wave, is also apparent for the TW moving past an edge. However, the latter type of wave can generate higher bending stresses than the full wave, with the exception of the range kl=0.34–1.0, where the TW and FW stresses are nearly equal. Below the value kl=0.34, the frontal peak stress predominates, which accounts for the change in shape of the TW curve.

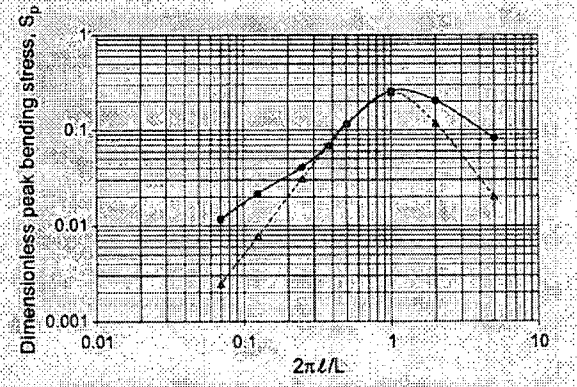

Fig. 5. Variation of peak bending stress with wave number (dimensionless forms). Circles: truncated wave advancing past an edge; triangles: full wave under infinitely long ice cover, without edge.

To determine what wavelengths are capable of fracturing an ice cover, one may calculate S_f, the absolute value of S that corresponds to the flexural ice strength σ_f. Using typical values of σ_f=600 kPa, E=7 GPa, h=0.5 m, l=9.5 m (from Eq. (3)), and w_0=0.1 m (low-amplitude wave), S_f works out to be 0.16. Inspection of Fig. 5 indicates that S_p exceeds S_f within the range kl=0.6–2.0. This translates to wavelengths L=30–100 m. For much thinner or weaker covers, the value of S_f will be less than 0.16, so that the above range will expand accordingly (note that $S_f \propto \sigma_f\sqrt{h}$, since $l \propto h^{3/4}$).

The spacing of cracks can be obtained from the variation of ξ_p, the dimensionless coordinate of the peak stress ($\xi_p=x_p/l\sqrt{2}$, with x_p=distance of peak stress location from the ice edge). This variation is depicted in Fig. 6, along with the relationship that would apply if x_p were equal to the wavelength L. The spacing of cracks is less than L at all wavelengths studied, although this might be reversed for very short waves (kl>6 or so).

Within the range kl=0.6–2.0, ξ_p is between 1.3 and 3.8. Consequently, the crack spacing x_p is expected to be between 1.8l and 5.4l, which translates to 20–50 m for an ice thickness of 0.5 m, or 40–100 thicknesses. Of course, these figures will change if the cover is weaker or thinner, but not sufficiently to alter the essential conclusion that the crack spacing is in the order of tens of ice thicknesses. A similar result has

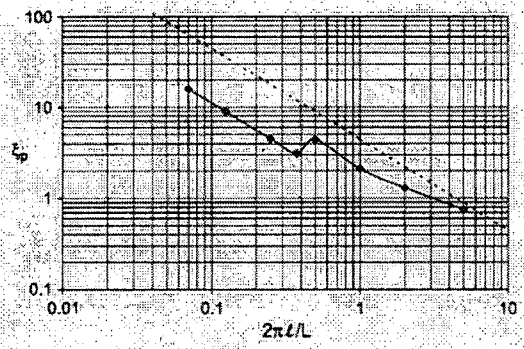

Fig. 6. Variation of dimensionless crack spacing with dimensionless wave number for truncated waves. The dotted line represents the dimensionless wavelength.

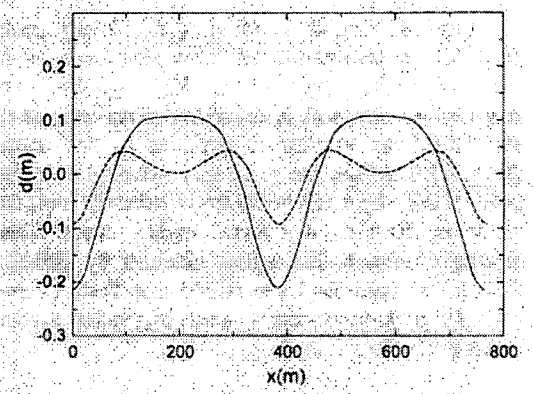

Fig. 7. Cnoidal wave forms calculated by Xia and Shen (2002).

been obtained for high-amplitude monoclinal waves, representing the rising limb of surges form ice jam releases (Billfalk, 1982; Beltaos, 1985, 1990).

6. Discussion

So far, the present analysis has been based on the familiar sinusoidal waves that result from linearization of the equations of motion. The limited evidence that is available to date (Beltaos and Rowsell, 2001) suggests that the sinusoidal function provides a fair approximation to measured low-amplitude wave forms. On the other hand, Xia and Shen (2002) calculated that nonlinear waves, known as cnoidal, could also generate sufficient stresses to fracture the ice cover. The cnoidal wave consists of steep troughs separated by long, relatively flat peaks, as illustrated in Fig. 7. The peak stresses are generated by the troughs where curvature is maximized.

Although the cnoidal wave is expressed by very complex mathematical functions, the trough shape can be approximated by a sinusoidal function over a considerable distance from the bottom of the trough. For instance, the wave represented by the solid line in Fig. 7 is very closely matched within the first 70 m by a cosine function with L=290 m (Fig. 8). This corresponds to kl~0.22 (l~10 m for h~0.5 m), which is within the range of wavelengths where the peak stress occurs just ahead of the leading edge, and when the wave has advanced past the edge by a quarter of the wavelength. The crack spacing can thus be obtained from Fig. 6 as $5\sqrt{2}l$ or 70 m. This is much less than 390 m, the length of the cnoidal wave (Fig. 7).

In general, therefore, it is concluded that bending of an ice cover by low-amplitude water waves can only produce closely spaced cracks in the order of tens of ice thicknesses. One may be tempted to extrapolate the present results to high-amplitude waves, such as may result from ice jam releases, by using a large value for the wave amplitude w_0. This would be incorrect, however, because ice jam-generated surges do not resemble the convex sinusoidal function depicted in Fig. 4c, but exhibit concave forms, culminating in a relatively sharp peak. At the same time, previous work has shown that the spacing of cracks that may be generated by such waves also amounts to tens of ice thicknesses (Billfalk, 1982; Beltaos, 1990).

Few observations of cracks with the predicted magnitude of spacing have been reported in the

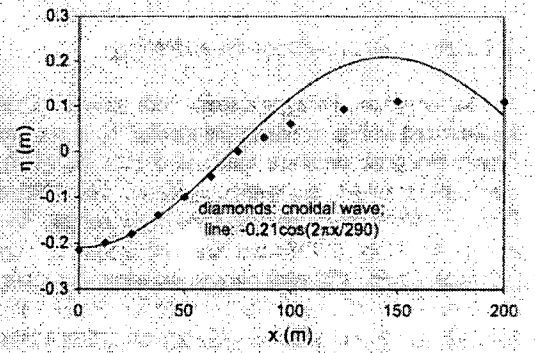

Fig. 8. Approximation of cnoidal wave trough with a cosine function; L=290 m.

literature. Parkinson (1982) described an episode of widespread fracture on the Liard River, producing visually estimated crack spacing between 50 and 200 m in an ice cover slightly thicker than 1 m. The cracks were both transverse and longitudinal in orientation, and most likely appeared during the passage of a surge. The lower end of the range is in agreement with the present findings, whereas the higher end is not. Parkinson's description suggests a highly dynamic process and movement of the ice cover, so that ice-to-ice interactions may have also played a role. The same applies to the longitudinal cracks, which cannot be explained by laterally uniform waves.

The writer has also observed surge-related closely spaced cracks (~50 m) on the Saint John River (1993 breakup; see photo in Fig. 9) and Restigouche River (2000 breakup), but only fleetingly: on both occasions, ice and water were moving far too swiftly for any kind of measurement beyond visual estimates by scaling crack spacing on the width of the river.

The relatively close spacing of wave-generated cracks greatly facilitates dislodgment and movement of the winter ice cover. As described by Beltaos (1997), ice movement occurs when the rising river stage creates sufficient surface clearance to allow passage of the individual ice sheets that are produced by transverse cracks. Usually, such cracks are spaced at hundreds or thousands of ice thicknesses, and are caused by bending on horizontal planes. Ice sheets of this length require considerable stage increases above the preceding freezeup level before they can be mobilized. Wave-generated ice sheets, on the other hand, are much shorter and require minimal stage increases. Coupled with the considerable surge height and the large shear stress that typically accompany a surge, this effect explains the well-known potential of surges for creating "sheet ice breakup fronts" (Jasek, 2003).

7. Summary and conclusions

Earlier work on the flexure of a river ice cover by transverse, low-amplitude water waves has been based on the assumption of an infinitely long wave propagating under an infinitely long and "edgeless" ice cover. This configuration does not need to account for the structural edge conditions of zero bending moment and shearing force and, hence, permits derivation of exact analytical solutions of the PDE describing ice response to a periodic load that results from the water wave.

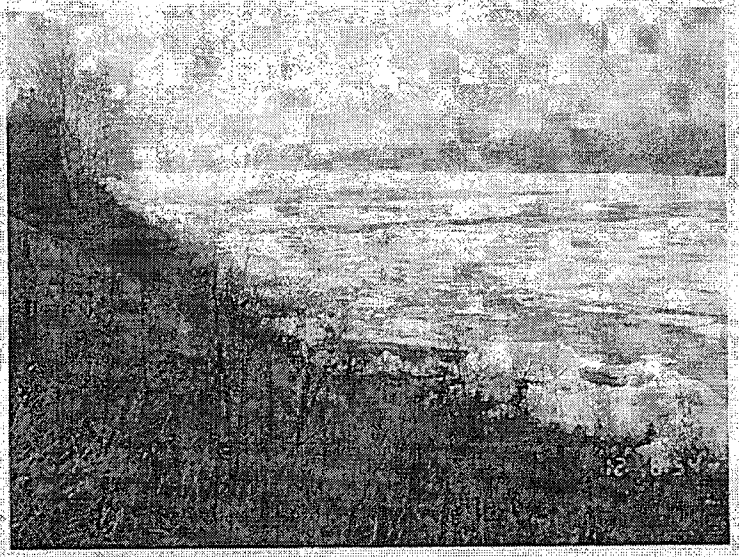

Fig. 9. Moving ice sheets in Saint John River near Ste-Anne de Madawasca, NB, during passage of a surge on April 12, 1993. A jam located 7 km upstream had released 15 min earlier.

However, such solutions are realistic if there is no ice edge nearby. Since any wave-generated cracks are structurally equivalent to edges, it is necessary to examine the effects of edge proximity on the response of the ice cover, not only for a full water wave (extending to infinity) but also for a TW (i.e., one that has only advanced a limited distance past the edge or crack). In addition to stating the wave fracture problem in more realistic terms, this approach also addresses the question of the crack spacing, which has been a matter of some ambiguity in the past. Noting that the inertial term is negligible, the ice response PDE is simplified and solved approximately via superposition of numerous concentrated loads. An analytical solution is also obtained for a wave that has advanced very far from the edge without generating cracks. This solution illustrates edge effects and serves as a check on the accuracy of superposition results.

The results indicate that, other things being equal, a truncated low-amplitude wave, which is a wave propagating past an edge (or crack) into a an undisturbed region, produces generally higher bending stresses than does an infinitely long wave propagating under an edgeless cover. However, the maximum possible stress is the same for both cases, and occurs at the same dimensionless wave number of 1, or where the wavelength is equal to about six times the characteristic length of the ice cover. The distance of the peak bending stress from the edge, which defines the spacing of cracks, varies with wavelength and is less than 100 ice thicknesses or so. This magnitude is comparable to that of high-amplitude, single waves (or surges) that result from ice jam releases. In fact, it is during such surges that this type of fracture has been observed to date, which helps explain the ice-clearing capacity of the surge.

Appendix A. Order-of-magnitude analysis: Eq. (4)

To compare the magnitudes of the three terms on the LHS of Eq. (4), we first note that, for a wave form that moves unchanged with celerity C, the time derivative is simply related to the spatial derivative via:

$$\frac{\partial \eta}{\partial t} = -C\frac{\partial \eta}{\partial x} \tag{A.1}$$

The order of magnitude of a spatial derivative can be expressed as $O(\partial\eta/\partial x)=\eta_0/pL$, in which η_0 is the maximum value of the absolute ice deflection, and p is a fraction defining the part of the wavelength that contains the distance between a peak or trough and the nearest point where the ice deflection becomes zero. For instance, a sinusoidal wave will have $p=1/4$, whereas a cnoidal wave, such as those in Fig. 5, would have $p \approx 1/5$. Noting that the third term (η) is in the order of η_0, the relative orders of the first and second terms can be written as:

$$O\left(\frac{s_i h}{g\eta}\frac{\partial^2 \eta}{\partial t^2}\right) = \frac{hC^2}{g\eta}\frac{\partial^2 \eta}{\partial x^2} = \frac{hC^2}{gp^2L^2} \tag{A.2}$$

and

$$O\left(\frac{l^4}{\eta}\frac{\partial^4 \eta}{\partial x^4}\right) = \frac{l^4}{p^4L^4} \tag{A.3}$$

With reference to Fig. 1, Eq. (A.2) can be used to show that the vertical ice acceleration term is negligible relative to the ice deflection η (see also Eq. (4)) for moderate and large wavelengths ($L \geq 2\pi l$), which cover the kinematic, dynamic, and gravity ranges. For shorter waves ($L < 2\pi l$), the ice stiffness term becomes very large (Eq. (A.3)). Using the wave celerities predicted by Daly (1995) for the ice-coupled and acoustic ranges ($L \leq 2\pi l$), it can be shown that the inertial term is now much smaller than the stiffness term, with the possible exception of the upper portion of the ice-coupled range.

The celerities indicated in Fig. 1 derive from the linearized analysis, which requires that the wave amplitude be small enough, relative to water depth, to render nonlinear terms negligible (Daly, 1993). The less restrictive nonlinear analysis of Xia and Shen (1999, 2002), which results in a cnoidal wave, predicts a wave celerity that is slightly less than, or equal to, that of a linear gravity wave ($\sqrt{gy}$). Substituting $C=\sqrt{gy}$ in Eq. (A.2) gives:

$$O\left(\frac{s_i h}{g\eta}\frac{\partial^2 \eta}{\partial t^2}\right) = \frac{hy}{p^2L^2} \tag{A.4}$$

With plausible values for h and y (~0.5 and 5 m, respectively), the range of wavelengths discussed by Xia and Shen (60–440 m) results in negligible (relative to 1) values for the RHS of Eq. (A.4).

It can thus be concluded that the neglect of the inertial term is justified for both linear and nonlinear wave types.

References

Balmforth, N.J., Craster, R.V., 1999. Ocean waves and ice sheets. Journal of Fluid Mechanics 395, 89–124.

Beltaos, S., 1985. Initial fracture patterns of river ice cover. National Water Research Institute contribution 85-139, Burlington, 51 pp.

Beltaos, S., 1990. Fracture and breakup of river ice cover. Canadian Journal of Civil Engineering 17 (2), 173–183.

Beltaos, S., 1995. Breakup of river ice. National Water Research Institute contribution 95-125, Burlington, 88 pp. In: Shen, H.T. (Ed.), Prepared as Chapter 5 for "River Ice Processes and Hydraulics". IAHR.

Beltaos, S., 1997. Onset of river ice breakup. Cold Regions Science and Technology 25 (3), 183–196.

Beltaos, S., 1998. Scale effects on river ice fracture and breakup. Proceedings, 14th International Ice Symposium, Potsdam, NY, USA, July 1998, vol. 1, pp. 631–636.

Beltaos, S., Krishnappan, B.G., 1982. Surges from ice jam releases: a case study. Journal of Civil Engineering 9 (2), 276–284.

Beltaos, S., Rowsell, R., 2001. Field study of pre-breaku p river waves. Proceedings (Available in CD Format), 11th Workshop on River Ice, Ottawa, pp. 4–17.

Billfalk, L., 1982. Break-up of solid ice covers due to rapid water level variations. U.S. Army CRREL Report 82-3, Hanover, NH, USA, 24 pp.

Daly, S.F., 1993. Wave propagation in ice-covered channels. ASCE Journal of Hydraulic Engineering 119 (8), 895–910.

Daly, S.F., 1995. Fracture of river ice covers by river waves. Journal of Cold Regions Engineering, ASCE 9 (1), 41–52.

Gold, L.W., 1971. Use of ice covers for transportation. Canadian Geotechnical Journal 8 (2), 170–181.

Henderson, F.M., Gerard, R., 1981. Flood waves caused by ice jam formation and failure. Proceedings of the IAHR Symposium on Ice, Quebec, Canada, vol. 1, pp. 277–287.

Hetenyi, M., 1946. Beams on elastic foundation. The University of Michigan Press, Ann Arbor, Mi., USA; also John Wiley & Sons Canada, Rexdale, Canada.

Hicks, F.E., 2003. Modelling the interaction of climate, hydrology and river ice hydraulics Mackenzie GEWEX study (MAGS) Phase 2. Proceedings, 8th Scientific Workshop, Jasper, AB, November 6–8, 2002, pp. 151–161.

Jasek, M., 2003. Ice jam release surges, ice runs, and breaking fronts: field measurements, physical descriptions, and research needs. Canadian Journal of Civil Engineering 30 (1), 113–127.

Parkinson, F.E., 1982. Water temperature observations during breakup on the Liard–Mackenzie River system. In: Andres, D.D., Gerard, R. (Eds.), Proceedings of the Workshop on Hydraulics of Ice-Covered Rivers, National Research Council of Canada, pp. 261–290.

Ponce, V.M., Simons, D.B., 1977. Shallow wave propagation in open channel flow. Journal of the Hydraulics Division, ASCE 103 (HY12), 1461–1476.

Steffler, R.M., Hicks, F.E., 1994. Discussion of "Wave propagation on ice-covered channels". ASCE Journal of Hydraulic Engineering 120 (12), 1478–1480.

Xia, X., Shen, H.T., 1999. Interaction of shallow water waves with ice cover. Report 99-3, Department of Civil and Environmental Engineering, Clarkson University, Potsdam, NY, USA.

Xia, X., Shen, H.T., 2002. Nonlinear interaction of ice cover with shallow water waves in channels. Journal of Fluid Mechanics 467, 259–268.

PRINTED IN CANADA
IMPRIMÉ AU CANADA
ON RECYCLED PAPER
SUR DU PAPIER RECYCLÉ

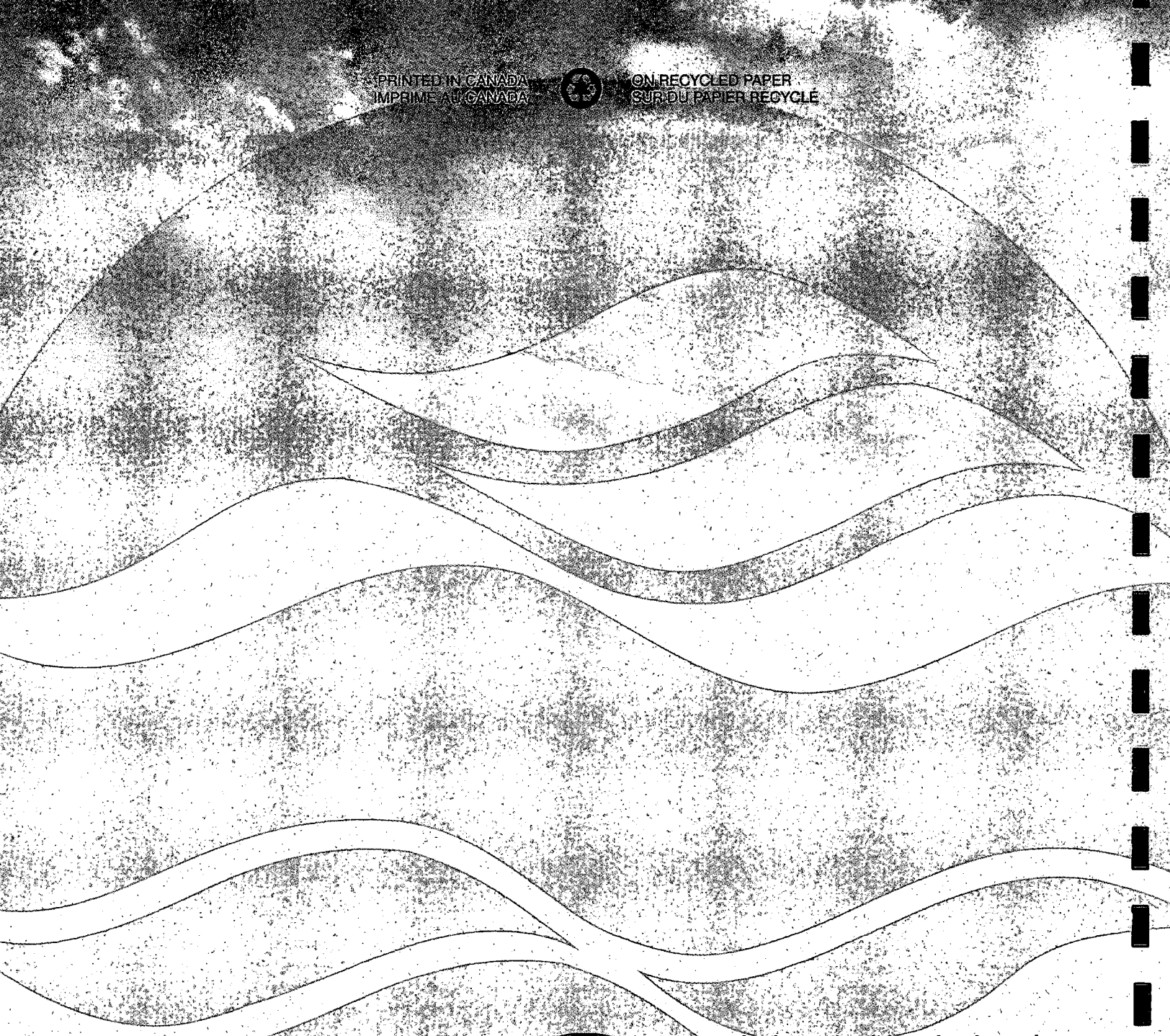

National Water Research Institute
Environment Canada
Canada Centre for Inland Waters
P.O. Box 5050
867 Lakeshore Road
Burlington, Ontario
L7R 4A6 Canada

National Hydrology Research Centre
11 Innovation Boulevard
Saskatoon, Saskatchewan
S7N 3H5 Canada

NATIONAL WATER RESEARCH INSTITUTE
INSTITUT NATIONAL DE RECHERCHE SUR LES EAUX

Institut national de recherche sur les eaux
Environnement Canada
Centre canadien des eaux intérieures
Case postale 5050
867, chemin Lakeshore
Burlington, Ontario
L7R 4A6 Canada

Centre national de recherche en hydrologie
11, boul. Innovation
Saskatoon, Saskatchewan
S7N 3H5 Canada

Environment Canada Environnement Canada

Canada